MULTIVARIATE GEOSTATISTICS: BEYOND BIVARIATE MOMENTS

FELIPE B. GUARDIANO and R. MOHAN SRIVASTAVA[1]
Applied Earth Sciences Department, Stanford, CA, USA, 94305

Traditionally, geostatistical models are conditioned only on univariate and bivariate statistics such as the sample histogram and covariance or indicator covariances. Higher order sample statistics such as three, four, multi-point covariances, as obtained, for example, from a training image, would improve considerably stochastic images if they could be reproduced.

An extended concept of indicator kriging allows the production of images that honor any number of multiple-point indicator covariances representing multiple-event experimental frequencies. The technique is applied to the stochastic imaging of phenomena sparsely sampled with complex features that cannot be captured by two-point statistics.

INTRODUCTION

In geostatistics, characterization of uncertainty about a spatially distributed phenomenon is done through conditional simulation. Conditional simulation consists of generating realizations of a random function (RF) conditioned by certain structural information, usually a univariate cumulative distribution function (cdf) and moments of the bivariate distribution such as the attribute covariance or some indicator covariances. Higher order statistics, such as the trivariate, quadrivariate, multiple-point distributions, are imposed by the implicit or explicit RF model, and by conditioning the realizations to local data. There are situations where available data allows the inference of these higher order statistics and one would wish to impart those statistics to the stochastic images. The algorithm proposed here allows for the explicit reproduction of such multiple-point statistics, generating realizations that reflect more accurately the spatial features of the underlying phenomenon.

Consider as an introductory example, the top image of Figure 1. It shows a section of a cross-bedded aeolian sandstone imaged with black and white pixels. The black pixels correspond to very fine sediments. Their tight horizontal connectivity would create low vertical permeability flow barriers in a reservoir. Note the typical dune-like curvilinear shape of the black pixel patterns. The white pixels correspond to

[1]also with FSS International, Vancouver, BC

A. Soares (ed.), *Geostatistics Tróia' 92*

coarser higher permeability sediments. An accurate appraisal of the flow behaviour of such sedimentary sequences would require a good characterization of the spatial arrangement of the fines.

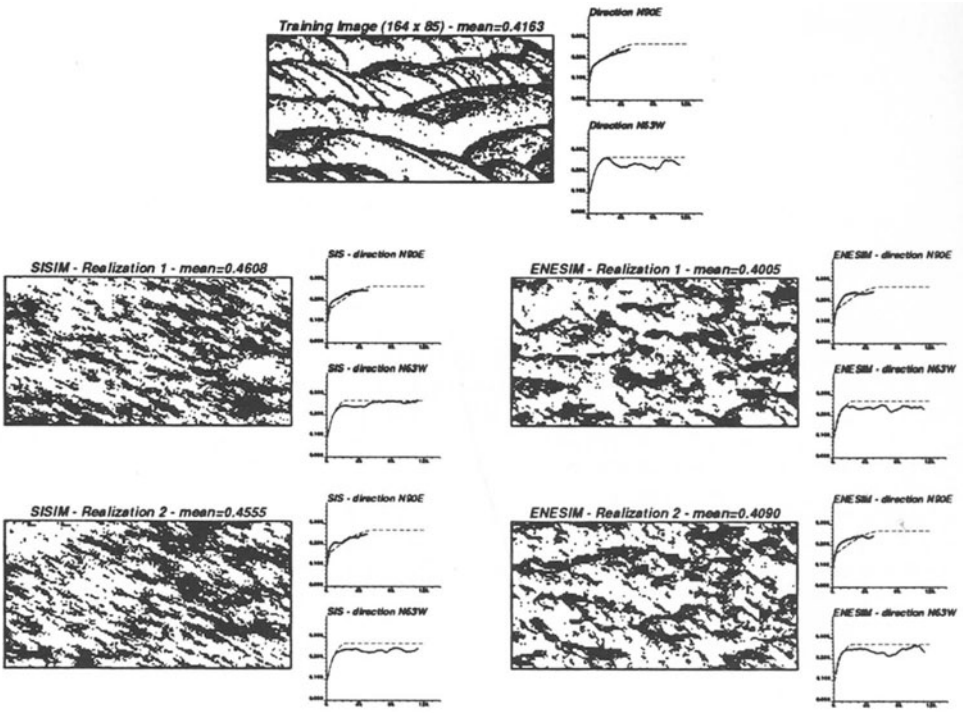

Figure 1: *Stochastic imaging of cross-bedded sand. The reference image (*165×84 *pixels) is shown on the top. The two images on the left are realizations produced by sequential indicator simulation (SISIM); the two images on the right are produced by the new proposed extended normal equations simulation (ENESIM) algorithm. All four images are shown to reproduce correctly the univariate and bivariate indicator statistics of the training image.*

The training image at the top of Figure 1 comprises 164 x 85 = 13,940 pixels, 42% of them being black. 73 samples, i.e. about one half of a percent of the training image, were collected at random to be used as conditioning data (sample proportion of black pixels is 47%). In addition, the exhaustive indicator semivariograms in the directions EW (*horizontal*) and N63W were retrieved from the training image. The latter direction corresponds to that of the longer right limb of the dune-shaped black pixels.

Although simplistically binary, the essential features of the training image defy reproduction using the traditional two-point statistics (here an indicator variogram model). The two lower left images of Figure 1 are reproductions honoring the previous univariate and bivariate indicator statistics; yet they fail to *look like* the training

image, in particular the characteristic curvilinear dune shape has not been reproduced. These two lower left images are two independent realizations of an indicator RF model $I(\mathbf{u})$, defined as:

$$I(\mathbf{u}) = \begin{cases} 1 & \text{if } \mathbf{u} \text{ is a black pixel} \\ 0 & \text{if not} \end{cases} \quad (1)$$

and conditioned by the 73 sample data in addition to a variogram modeled from the two previous exhaustive indicator variograms. These realizations were obtained from sequential indicator simulation (SISIM) using routine `sisim` of the public domain software GSLIB (Deutsch and Journel, 1992).

Clearly, more than two-point statistics are necessary to account for the curvilinear dune-shaped pattern of black pixels seen on the training image. The same 73 sample data were used to produce the two independent realizations shown at the lower right of Figure 1. Here, the proposed extended normal equations (ENESIM) algorithm was used. Reproduction of the univariate (proportion of black pixels) and the indicator variograms is similar to that achieved by SISIM images. However, the ENESIM images start capturing the dune shape. The additional information provided to the ENESIM simulation algorithm is precisely multiple-point indicator covariances directly read from the training image, as described hereafter.

Note that the goal of any simulation is not to reproduce the training image. The objective is to generate realizations that account for (are constrained by) information deemed relevant to the underlying phenomenon. The training image itself is not the underlying phenomenon. It is assumed, however, that both share some structural properties such as specific multiple-point covariances.

BAYES' RELATION

The indicator formalism for evaluation of conditional probabilities, Journel and Alabert (1989), is actually a particular case and an approximation of a much more general and powerful concept of extended normal equation including Bayes' relation itself, Solow (1986). Consider any particular yet unobserved event A_0 whose conditional probability is to be assessed. The conditioning information is constituted by n data events A_α with $\alpha = 1, \ldots, n$. The event A_0 could be as simple as $Z(\mathbf{u}) \leq z$, indicating whether a particular unsampled continuous attribute value $z(\mathbf{u})$ is valued below threshold z or not, or it can involve multiple events at different locations such as a string of high values $A_0 : \{Z(\mathbf{u}) > z; \mathbf{u} \in \textit{string } L\}$. Similarly each of the data events A_α may be as simple as a single-location datum value $A_\alpha : \{Z(\mathbf{u}_\alpha) = z_\alpha\}$, or it can be as complex as the set of all data values $S(n) : \{Z(\mathbf{u}_\alpha) = z_\alpha, \alpha = 1, \ldots, n\}$.

More precisely, let the random variables A_0, A_α, and $S(n)$ be binary random variables, set to 1 if the corresponding event occurs, to 0 otherwise. The conditional probability of the event A_0 given the n data events $A_\alpha = 1$, $\alpha = 1, \ldots, n$, is equal to the conditional expectation of the indicator random variable A_0:

$$\begin{aligned} Prob\{A_0 = 1 \mid A_\alpha, \alpha = 1, \ldots, n\} &= E\{A_0 \mid S(n) = 1\} \\ &\equiv [A_0]^*_{SIK} = E\{A_0\} + \lambda[1 - E\{S(n)\}] \end{aligned} \quad (2)$$

with $[A_0]^*_{SIK}$ being the simple indicator kriging (SIK) estimate of A_0; $S(n) = \prod_{\alpha=1}^{n} A_\alpha$ is the single indicator of the global data event with $S(n) = 1$ if and only if all

elementary data events occur simultaneously, $A_\alpha = 1, \forall\, \alpha = 1, \ldots, n$. The system of normal equations is reduced to a single equation:

$$\lambda . Var\{S(n)\} = Cov\{A_0, S(n)\} \tag{3}$$

with:

$$\begin{aligned} Var\{S(n)\} &= E\{S(n)\}.[1 - E\{S(n)\}] \\ E\{S(n)\} &= Prob\{S(n) = 1\} = Prob\{A_\alpha = 1, \alpha = 1, \ldots, n\} \\ Cov\{A_0, S(n)\} &= E\{A_0.S(n)\} - E\{A_0\}.E\{S(n)\} \\ E\{A_0.S(n)\} &= Prob\{A_0 = 1, S(n) = 1\} \end{aligned}$$

Hence:

$$\begin{aligned} E\{A_0 \mid S(n) = 1\} &= E\{A_0\} + \frac{E\{A_0.S(n)\} - E\{A_0\}.E\{S(n)\}}{E\{S(n)\}} \\ &= \frac{E\{A_0.S(n)\}}{E\{S(n)\}} = \frac{Prob\{A_0 = 1, S(n) = 1\}}{Prob\{S(n) = 1\}} \end{aligned} \tag{4}$$

as given by Bayes' relation.

Indicator kriging with a single global data event is exact inasmuch as Bayes' postulate, itself at the basis of the notion of conditional probability. All that is required is inference of the probabilities of the ratio (4) or, equivalently, of the two indicator covariances $Var\{S(n)\}$ and $Cov\{A_0, S(n)\}$ required by the normal equation (3).

In the case of the exercise depicted in Figure 1, $A_0 = I(\mathbf{u})$ is the indicator of a black pixel at any unsampled location $\mathbf{u}_0$, and $S(n) = \prod_{\alpha=1}^{n} A_\alpha = 1$ represents the set of all 73 indicator data A_α all set to 1, i.e. such that:

$$A_\alpha = A(\mathbf{u}_\alpha) = \begin{cases} I(\mathbf{u}_\alpha) = 1 & \text{if } I(\mathbf{u}_\alpha) = 1 \\ 1 - I(\mathbf{u}_\alpha) = 1 & \text{if } I(\mathbf{u}_\alpha) = 0, \forall\, \alpha = 1, \ldots, n \end{cases} \tag{5}$$

Inference of the probability $E\{A_0.S(n)\} = E\{I(\mathbf{u}_0).\prod_{\alpha=1}^{n} A_\alpha\}$ calls for scanning the training image to evaluate the frequency of occurrence of the joint event $\{I(\mathbf{u}) = 1, A(\mathbf{u}+\mathbf{h}_\alpha) = 1, \alpha = 1, \ldots, n\}$ with $\mathbf{h}_\alpha = \mathbf{u}_\alpha - \mathbf{u}_0$, for the given geometric configuration of the $(n+1)$ locations $\mathbf{u}$, $\mathbf{u} + \mathbf{h}_\alpha$, $\alpha = 1, \ldots, n = 73$. Similarly, the probability $E\{S(n)\}$ would be inferred by the corresponding[2] frequency of occurrence of the global data event $\{\prod_{\alpha=1}^{n} A(\mathbf{u} + \mathbf{h}_\alpha) = 1\}$.

[2]The reader may have associated the choice of a particular training image to the decision of stationarity. For consistency, it is essential that the two experimental frequencies $E\{A_0.S(n)\}$ and $E\{S(n)\}$ be inferred from exactly the same set of $(n+1)$-tuples locations $\{\mathbf{u}, \mathbf{u}+\mathbf{h}_\alpha, \alpha = 1, \ldots, n\} \subset$ training image. This common set is called the *eroded* area of the training image by the specific configuration of the $(n+1)$-tuples considered. The larger n, the larger the distances $\mathbf{h}_\alpha = \mathbf{u}_\alpha - \mathbf{u}_0$, the smaller the eroded training image left for the inference process. The previous problem of consistency is at the root of questions of positive definiteness when modelling indicator covariances as required by normal equations of type (3).

SIMULATION

Once the relative frequency (4), i.e. $E\{A_0 \mid S(n) = 1\}$, is inferred, one can draw by Monte Carlo a realization for A_0. For example, if $E\{A_0 \mid S(n) = 1\} = 0.6$, the simulated value for A_0 is 1 whenever the uniform $[0,1]$ random number drawn is lesser than or equal to 0.6. Whatever the value simulated (0 or 1) for A_0 at location $\mathbf{u}_0$, it becomes a datum event for the next node $\mathbf{u}_0'$ to be simulated according to the sequential simulation principle, Deutsch and Journel (1992). Therefore, the global data event $S(n+1)$ for the next node $\mathbf{u}_0'$ is of dimension $n+1$. If N nodes are to be simulated with n original elementary data events, the global data event dimensions grows gradually from n for the first node being simulated to $(n+N-1)$ for the last node.

REDUCING THE INFERENCE PROBLEM

Although the general indicator kriging expression (2) or (4) is exact, it is not practical as soon as the number n of elementary data events becomes large, unless the training image is correspondingly very large. Indeed, as n grows, or if the global data event $S(n)$ is complex, it is unlikely to find on the training image enough $(n+1)$-tuple events such as $S(n) = 1$ to allow inference of the frequencies $E\{A_0.S(n)\}$ and $E\{S(n)\}$. The solution consists of:

- either reducing the number n and complexity (specificity) of the data events, which amounts to reduce the amount of information conditioning the probability $E\{A_0 \mid S(n) = 1\}$
- or model both frequencies $E\{A_0.S(n)\}$ and $E\{S(n)\}$ as functions of, say, the n parameters $\mathbf{h}_\alpha$ of the data configuration. This amounts to interpolate or extrapolate all needed frequencies from a few actually calculated frequencies.

The second alternative is that traditionally used when a two-point Z-covariance $Cov\{Z(\mathbf{u}), Z(\mathbf{u}+\mathbf{h})\}$ or an indicator covariance $Cov\{I(\mathbf{u}), I(\mathbf{u}+\mathbf{h})\}$ are modeled by fitting a curve through actually calculated experimental covariance values. Unfortunately, the modelling option is limited to low order covariances (univariate and bivariate), thus does not allow capturing high order statistics from the data. The first solution is that considered to generate the ENESIM images at the right of Figure 1.

THE ENESIM ALGORITHM

The ENESIM simulation algorithm proceeds as follows:

1 - Define a random path visiting all unsampled nodes of the simulation grid, in the case of Figure 1 all (13,940-73)=13,867 nodes discretizing the training image excluding the 73 conditioning data.

2 - At each node $\mathbf{u}_i$, retain the nearest $\frac{n}{4}$ conditioning indicator data (black or white) in each quadrant, for a total of n set to 16 in this exercise. Scan the

training image for all 17-tuples reproducing the node $\mathbf{u}_i$-to-16 data configuration, and evaluate the conditional probability (4). That conditional probability is retained only if there are at least a minimum number *min* (fixed at 20 for this exercise) of identical 17-tuples configurations. If not, the furthest away datum is dropped, reducing the data size to 15, and the training image is scanned again[3], etc ..., until the minimum required number of identical data configurations is found.

3 - From the conditional probability (4) draw a simulated value (black or white) for node $\mathbf{u}_i$. That simulated value is then coded as a datum value to be used for the conditional simulation of all subsequent nodes.

4 - Move to the next node $\mathbf{u}_{i+1}$ along the random path and repeat steps 2 and 3.

Loop until all the nodes are informed with a simulated value. One stochastic image has been generated. If another image is needed, reiterate the entire process from step 1.

The algorithm can be easily modified to retain preferentially specific data configurations (e.g. those revealing the characteristic dune shape) rather than the closest $\frac{n}{4}$ data in each quadrant. It can also be adapted to categorical indicator variables that can take more than 2 outcomes; beware though that if there are K categories and n data locations retained there may be up to K^n joint realizations of the n data values, e.g. $K^n = 1.5 \times 10^{11}$ for $K = 5$ and $n = 16$. Fortunately, if the original conditioning data are consistent with the training image statistics the actual data configuration and values retained at any node will be found often enough in the scanning process.

SIMULATION OF PORE GEOMETRY

The training image for this second case study, see Figure 2, is a digitized thin section of an oil bearing sand with shale clasts of different sizes and orientation (Kramers et al, 1989). Three families of shale sizes can be distinguished in this image. The shale are represented as black pixels and the white pixels represent the porous sand matrix through which fluids can flow.

The top image of Figure 2 serves as the phenomenon to be simulated. It comprises 116 x 59 = 6,844 pixels averaging 43% black. 47 pixels (black or white) are sampled from this top image for conditioning the stochastic imaging process, averaging 54% black.

Unlike the example of Figure 1, and as would be the case in most practical applications, the training image (second from top in Figure 2) is different from that to be simulated. However, both images share common structural traits if only because they were taken from the same sand facies. Indicator variograms for the two E-W and N-S directions were extracted from the training image and modeled.

The two lower left images of Figure 2 are two independent SIS realizations honoring the training indicator variogram model and the 47 conditioning data. They fail to

[3]Actually, all the frequencies corresponding to any subset of the initial 16 data configuration are embedded in the scanning made for that initial configuration.

reproduce the clast aspect of either the training or unknown image and would yield a much too low effective permeability: the black pixels are not disconnected into separate clasts.

The two lower right images of Figure 2 are two independent realizations of the ENESIM algorithm conditioned to the same 47 data but building from multiple-point statistics taken from the training image. The ENESIM implementation is identical to that described for Figure 1. The clast aspect of the training and unknown images is better reproduced, hence the flow characteristics (e.g. permeability) of those images would also be better reproduced. Note that the two-point indicator variogram model, although not explicitly considered by the ENESIM algorithm, are well reproduced.

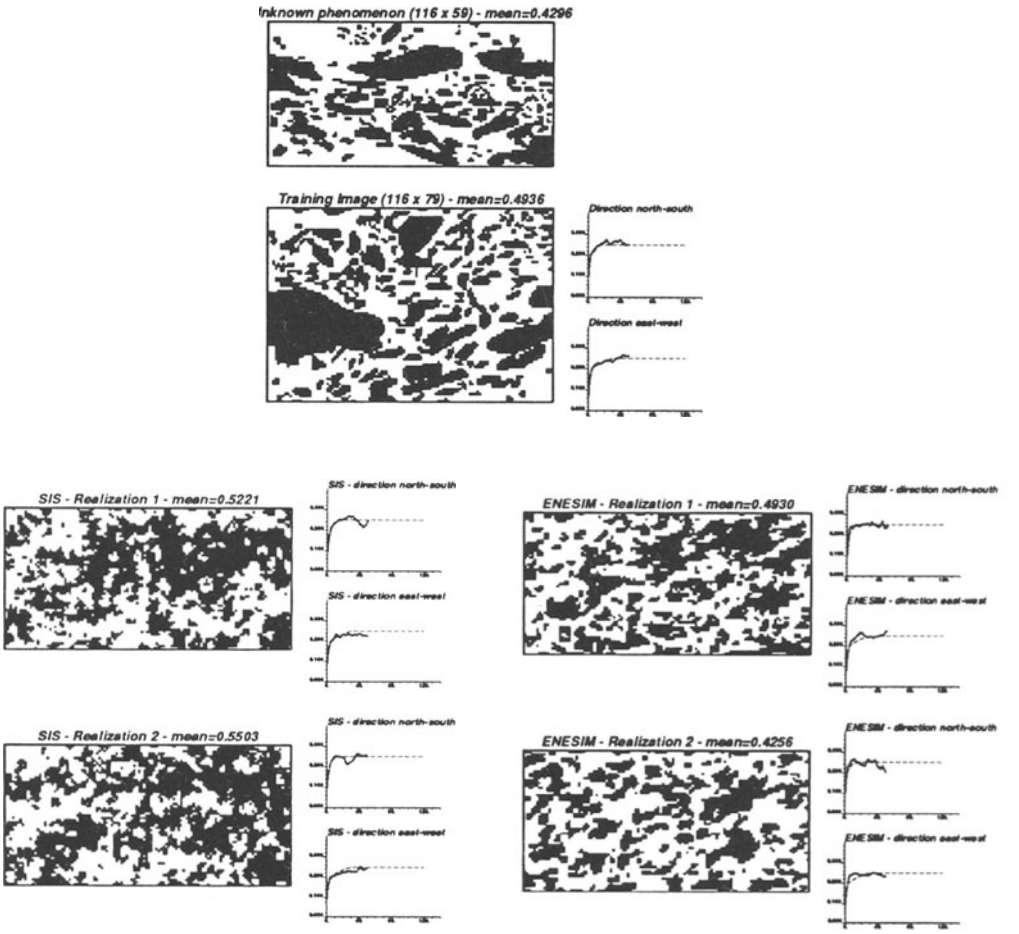

Figure 2: *The reference image to be reproduced is shown on the top. Below it is a training image taken from the same lithofacies. The two images at the lower left are realizations produced by SIS; the images at the lower right are produced by ENESIM. The experimental variograms shown to the right of each image correspond to directions north-south and east-west.*

Figure 3: *Both the conditioning data and the multiple-point statistics are taken from the same training image (second from the top on Figure 2) resulting in a much better reproduction of that training image.*

If the 47 conditioning data had been taken from the training image from which the multiple-point statistics are inferred, then a much better reproduction is achieved as shown by the two independent realizations of Figure 3. Once again, the reproduction of the training image indicator variograms (not shown) is excellent.

SIMULATION OF FRACTURE GEOMETRY

This third case study relates to the simulation of fracture distribution in carbonate rock. The image at the left of Figure 4 has been generated by an algorithm for physical crack propagation from initial (Poisson) seeds, Olson and Pollard (1989). That image has been digitized by 200 x 200 binary pixels (black or white) of which 22% were black. 200 conditioning data were taken at random averaging 23% black. These 200 data were used to condition the ENESIM realization at the right of Figure 4. The ENESIM realization averages 21% black and its indicator variograms in the two major directions EW and NS are shown to reproduce correctly the model fit from the exhaustive variograms derived from the training image. Once again, the ENESIM implementation is identical to that described for Figure 1.

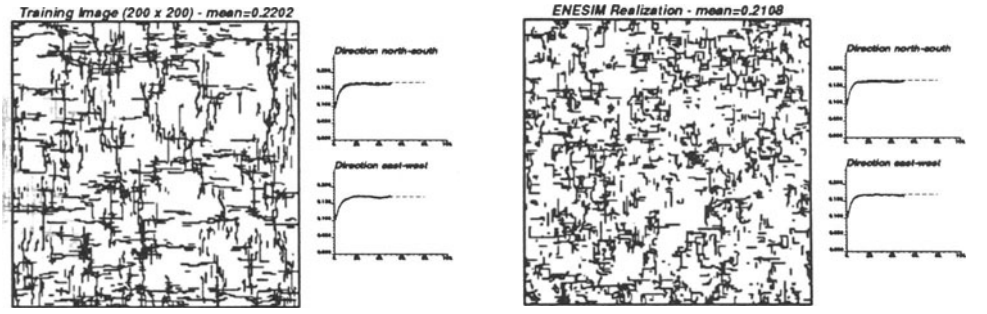

Figure 4: *The training image was generated by physical crack propagation. 200 data were extracted from it to condition the ENESIM realization shown at the right.*

One reason for the poor reproduction of the longer fracture lengths is the limitation to the nearest data found in each neighborhood: quickly in the sequential simulation algorithm these conditional data are very close to the node being simulated and fail to reflect the longer fracture lengths. A smarter search strategy could have been considered such as a neighborhood elongated along the north-south and/or east-west directions.

It is worth noting that the generation of the ENESIM realization using a prototype non-optimized code was about 10 times faster, cpu-wise, than the generation of the training image using the physical growth equations. If that training image is deemed representative of any other section of a 3D volume (isotropy), the ENESIM algorithm can easily expand that 2D training information into multiple 3D realizations, a task now beyond the capability of physical growth simulators.

Recall that the ENESIM simulation algorithm is exact, in that it honors the data values at their exact locations, no matter the density or configuration of these data. This exactitude condition is sometimes difficult to fulfill with Boolean algorithms which, in the case of Figure 4, would amount to drop at random fracture segments according to some prior length distribution. Such Boolean approach would have no control on the resulting indicator variogram.

EXTENDED NORMAL EQUATIONS

The single normal equation or Bayes' relation approach of equations (3) and (4) requires scanning a training image for frequencies related to a single global data event denoted $S(n)$ in these equations. Often such a training image is not available or is not extensive enough to allow reliable inference. One may then decompose that global data event $S(n)$ into simpler (less specific) information components whose related frequencies are easier to assess.

The global data event $S(n) = 1$ can be seen as anyone of 2^n joint realizations of the n elementary binary data events $A_\alpha, \alpha = 1, \ldots, n$, where A_α can take either values 0 or 1. The conditional probability (2) of event $A_0 = 1$ takes the more general expression (Cox, 1972; Journel and Alabert, 1989):

$$\begin{aligned} Prob\{A_0 = 1 \mid A_\alpha = a_\alpha, \alpha = 1, \ldots, n\} \;\equiv\; & [A_0]^*_{SIK} \\ = \;& \lambda_0 + \sum_{\alpha_1=1}^{n} \lambda^{(1)}_{\alpha_1} a_{\alpha_1} + \sum_{\alpha_1=1}^{n} \sum_{\alpha_2>\alpha_1}^{n} \lambda^{(2)}_{\alpha_1\alpha_2} a_{\alpha_1} a_{\alpha_2} \\ + \;& \sum_{\alpha_1=1}^{n} \sum_{\alpha_2>\alpha_1}^{n} \sum_{\alpha_3>\alpha_2}^{n} \lambda^{(3)}_{\alpha_1\alpha_2\alpha_3} a_{\alpha_1} a_{\alpha_2} a_{\alpha_3} + \cdots + \lambda^{(n)} \prod_{\alpha=1}^{n} a_\alpha \end{aligned} \tag{6}$$

The 2^n coefficients (IK weights) λ_0, $\lambda^{(1)}_{\alpha_1}$, $\lambda^{(2)}_{\alpha_1\alpha_2}$, $\lambda^{(3)}_{\alpha_1\alpha_2\alpha_3}$, ..., $\lambda^{(n)}$ are determined by an extended system of 2^n normal equations which establishes the orthogonality of the error vector $A_0 - [A_0]^*_{SIK}$ to the 2^n combination of data events $\mathbb{1}$, A_{α_1}, $A_{\alpha_1} A_{\alpha_2}$, ..., $\prod_{\alpha=1}^{n} A_\alpha$, see Projection Theorem (Luenberger, 1969). For example, consider the first normal equation expressing orthogonality of the error vector to the constant

unit vector $\underline{1}$, otherwise known as unbiasedness condition:

$$< A_0 - [A_0]^*_{SIK}, \underline{1} >= E\{A_0\} - \lambda_0 - \sum_{\alpha_1=1}^{n} \lambda^{(1)}_{\alpha_1} E\{A_{\alpha_1}\} - \ldots - \lambda^{(n)} E\{\prod_{\alpha=1}^{n} A_\alpha\} = 0 \quad (7)$$

This equation allows rewriting the ccdf (6) into the more familiar IK format:

$$Prob\{A_0 = 1 \mid A_\alpha = a_\alpha, \alpha = 1, \ldots, n\} \quad - \quad E\{A_0\}$$

$$= \sum_{\alpha_1=1}^{n} \lambda^{(1)}_{\alpha_1} [A_{\alpha_1} - E\{A_{\alpha_1}\}] + \sum_{\alpha_1=1}^{n} \sum_{\alpha_2>\alpha_1}^{n} \lambda^{(2)}_{\alpha_1\alpha_2} [A_{\alpha_1}.A_{\alpha_2} - E\{A_{\alpha_1}.A_{\alpha_2}\}] + \cdots$$

$$+ \quad \lambda^{(n)} [\prod_{\alpha=1}^{n} A_\alpha - E\{\prod_{\alpha=1}^{n} A_\alpha\}] \quad (8)$$

Expression (8) identifies expression (4), i.e. Bayes' relation, when the global data realization $S(n)$ corresponds to all switches a_α set to 1.

The traditional IK approximation amounts to retaining only the $(n+1)$ first terms of the expansion (6) or the n first terms of expansion (8). What is lost is the information carried by multiple joint data events such as $A_{\alpha_1}A_{\alpha_2}$ or $A_{\alpha_1}A_{\alpha_2}A_{\alpha_3}$. What is gained is easier inference: all that is needed are (traditional) two-event indicator covariances such as $E\{A_0.A_\alpha\}$ or $E\{A_\alpha.A_\beta\}$, $\forall\ \alpha, \beta = 1, \ldots, n$.

Availability of the full (and exact) expansion (8) allows retaining any number of combinations (products) of data events up to all $(2^n - 1)$ of them, depending on their information content and on the feasibility of the inference of the corresponding indicator covariances. For example, one may retain the partial IK estimate:

$$E^*\{A_0 \mid S(n) = 1\} \quad = \quad E\{A_0\} + \sum_{\alpha=1}^{n} \nu^{(1)}_\alpha [a_\alpha - E\{A_\alpha\}]$$

$$+ \quad \nu^{(2)}_{12} [a_1 a_2 - E\{A_1.A_2\}] \quad (9)$$

if the joint occurrence A_1A_2 (equal to 1 or 0) is deemed an information critical to the event A_0 to assess. The estimator (9) requires inference of the three-event indicator covariances $E\{A_0.A_1.A_2\}$ and $E\{A_\alpha.A_1.A_2\}$, $\alpha = 3, \ldots, n$, in addition to the traditional two-event indicator covariance $E\{A_\alpha.A_\beta\}$, $\alpha, \beta = 1, \ldots, n$.

The main contribution of the general indicator formalism is the possibility of considering any combination of data events of any type. For example, the elementary data events A_α can be:

- hard measurements made on the primary variable, A_α : $\{Z(\mathbf{u}_\alpha) = z_\alpha\}$
- constraint intervals, A_α : $\{Z(\mathbf{u}_\alpha) \in (a_\alpha, b_\alpha]\}$
- categorical data, A_α : $\{\mathbf{u}_\alpha \in facies\ k\}$

- prior (pre-posterior) probability distribution values such as A_α : $\{Prob\{Z(\mathbf{u}_\alpha) \leq z \mid Y(\mathbf{u}_\alpha) = y_\alpha\}$ where the distribution of the primary value $Z(\mathbf{u}_\alpha)$ is constrained by the information brought by the collocated secondary datum $Y(\mathbf{u}_\alpha) = y_\alpha$. That prior local cdf could be obtained by calibration from a scattergram of $z - y$ values, Zhu and Journel (1992).

- any multiple-event (point) information such as A_α : $\{Z(\mathbf{u}_\alpha + \mathbf{h}_\beta) \leq z_\beta, \beta = 1, \ldots, n_\alpha\}$

The limitation is not theoretical (the corresponding extended normal equations are easily written), it lies in the inference of the corresponding indicator covariances. The larger the number (n) of elementary data events and the more complex these data events (including soft information), the larger the training image or data set needed for inference. Problems of inconsistency arise if that inference is done from possibly different and partially inconsistent training data sets. These problems can be fixed in various *ad hoc* ways; this is the price to pay for using more and more relevant information.

CONCLUSIONS

Reconstruction of sparsely sampled phenomena must capitalize on ancillary structural (pattern) information that can be collected from similar fields better sampled (a training image). There is much more valuable information to collect from such a training image than two-point statistics most often limited to a mere covariance/variogram function (linear correlation). Important characteristic features of training images are often curvilinear and involve multiple points; the modeling and exportation of such features are well beyond the flexibility of traditional random function models.

The extended normal equations (indicator kriging) formalism allows capturing such multi-point statistics and using them for deriving more accurate probability distributions for the unknown events to be assessed. Conditioning can be done on very complex data events involving several locations jointly, and hard as well as soft measurements. The only requirement is that the relation (covariance) between these data events and the event to be assessed can be inferred from the training image. A more accurate conditional probability distribution reflects immediately into more accurate stochastic images or conditional simlations.

The algorithm calls for a brute-force, computer-intensive approach to inference and image reconstruction (stochastic imaging) characteristic of many modern engineering and mathematical fields.

REFERENCES

1 - Cox, D. R. (1972) *The analysis of multivariate binary data*, in Applied Statistics, **21** (2): 113-120.

2 - Deutsch, C. V. and Journel, A. G. (1992) *GSLIB: Geostatistical software library and User's Guide*, to be published by Oxford University Press.

3 - Journel, A. G. and Alabert, F. A. (1989) *Non-Gaussian data expansion in the earth sciences*, Terra Nova, **1** (2): 123-134.

4 - Kramers, J. W., Bachu, S., Cuthiell, D. L., Prentice, M. E. and Yuan, L. P. (1989) *A multidisciplinary approach to reservoir characterization: the Provost Upper Manville B Pool*, in Journal of Can. Pet. Tech., **28** (3): 1-11.

5 - Luenberger, D. (1969) *Optimization by vector space methods*, Wiley & Sons, 326 pages.

6 - Olson, J. and Pollard, D. (1989) *Inferring paleostresses from natural fracture patterns: A new method*, in Geology, **17**: 345-348.

7 - Solow, A. (1986) *Mapping by simple indicator kriging*, Math Geology, **18** (3): 335-352.

8 - Zhu, H. and Journel, A. G. (1992) *Formatting and integrating soft data: Stochastic imaging via the Markov-Bayes algorithm*, in Proc. of 4th International Geostatistical Congress (this volume).